

Chapter 8

Towards Long-Lasting Disaster Mitigation Following a Mega-landslide: High-Definition Topographic Measurements of Sediment Production by Debris Flows in a Steep Headwater Channel

Yuichi S. Hayakawa, Fumitoshi Imaizumi, Norifumi Hotta,
and Haruka Tsunetaka

Abstract Mega-landslides usually cause long-lasting subsequent sediment production, and long-term strategies for disaster mitigation are necessary in the case of such extreme events. The Ohya-kuzure landslide in central Japan is typical of sites where hillslope erosion and sediment yield have been continuously active since its formation in 1707. Sediment production is particularly active by debris flows in the headwater channels formed within the landslide. However, the dynamics of such debris flows in steep headwater channels have not been fully examined compared to those in gentler downstream reaches. To investigate the changes in headwater channel bed sediments remobilized mainly by frequent debris flows, repeated high-resolution measurements were carried out using terrestrial laser scanning. Freeze-thaw weathering in the surrounding slopes, which are composed of deformed shale and sandstone layers, delivers quantities of small particles onto the valley floor. Measurements in spring, summer, and autumn conducted over two years provided high-definition (0.1 m resolution) topographic datasets, revealing the seasonal amount of erosion and deposition to be on the order of 1000–5000 m³. Erosion and deposition along the reach also showed contrasting spatial patterns according to the sections bounded by knickpoints and valley narrows. These basic estimates of sediment production in headwater channels can be utilized for further mitigation of possible sediment-related disasters in downstream areas.

Y.S. Hayakawa (✉)

Center for Spatial Information Science, The University of Tokyo, Kashiwa, Japan
e-mail: hayakawa@csis.u-tokyo.ac.jp

F. Imaizumi

Faculty of Agriculture, Shizuoka University, Shizuoka, Japan
e-mail: imaizumi@cii.shizuoka.ac.jp

N. Hotta • H. Tsunetaka

Life and Environmental Sciences, University of Tsukuba, Tsukuba, Japan
e-mail: hotta.norifumi.ge@u.tsukuba.ac.jp; tsunetakaharuka@gmail.com

Keywords Debris flow • Steep terrain • Terrestrial laser scanning • Sediment disaster • High-definition topography • Landslide

8.1 Introduction

Compared to small- to medium-sized mass movement features, mega-landslides ($>10^7 \text{ m}^3$) caused by episodic triggers, such as extreme rainfall events and earthquakes, are relatively rare in human history (Keefer 1999; Korup et al. 2007; Korup 2012). Clearly such events are extremely hazardous at the time of their occurrence. Moreover, mega-landslides are potentially hazardous for a long time subsequent to their initial formation, due to continuous sediment yield that produces significant ongoing hazards downstream, impacting settlements and infrastructure along the river over distances far beyond the original slope failure location. Long-term strategies for disaster mitigation are therefore necessary in the case of such extreme events. However, the nature of sediment delivery by debris flows in unstable steep terrains after mega-landslides has not been fully examined. Lake sediments can record such historical sediment yields from upstream landslides over hundreds to thousands of years (Trustrum et al. 1999), although such an ideal situation is not always available particularly in urbanized areas.

The Ohya-kuzure landslide in central Japan is typical of landslide sites; in this case, erosion of hillslopes and sediment yield have been continuously active since its formation, about three centuries ago (Fig. 8.1). The earthquake-induced landslide is located in the uppermost region of a tributary of the Abe-kawa River, and the main channel was filled with abundant sediment immediately after the occurrence of the landslide. This caused significant hazards in the area, whereby channel avulsion caused a new course of the main stream to form a waterfall, and dammed lakes were reportedly formed (Fig. 8.1). After some time, incision into this sediment resulted in fill terraces along the main stream at heights of tens of meters above the channel bed. Even after centuries, sediment transportation remains active due to debris flows in headwater channels in the landslide (Tsuchiya and Imaizumi 2010). Very considerable erosion control efforts, known as “sabo” work (Ministry of Construction 1988), have been applied to the landslide area to stabilize the slopes and to prevent damage by debris flows (Fig. 8.2).

However, the physical dynamics of such debris flows in steep headwater channels have not fully been examined compared to those in gentler downstream reaches, partly due to limited access to such remote areas. Acquiring detailed data of topographic changes is one of the challenging issues for the study of debris flows in steep headwater channels. Even basic estimates of sediment production volumes, which are crucial for mitigation of possible sediment-induced disasters in the downstream areas, are difficult to obtain. Remote sensing approaches, such as aerial photography and laser scanning, are more efficient methods of performing such measurements (Imaizumi et al. 2005, 2006; Higuchi et al. 2012). However, both spatial and temporal resolutions are often insufficient to precisely capture the



Fig. 8.1 An old pictorial map showing the Ohya-kuzure landslide triggered by the Hoei earthquake in 1707. This map was drawn in 1863, and the changes in the location of villages and roads, as well as newer landslides after the Ohya-kuzure landslide are shown

frequent changes in topography by recurring debris flows. Terrestrial laser scanning (TLS) is one of the most efficient approaches to measuring topographic changes in steep channels and landslides (e.g., Rowlands et al. 2003; Teza et al. 2007). In this study, TLS was utilized for repeated measurements of valley-bottom deposits to investigate the changes in headwater channel bed sediments remobilized mainly by frequent debris flows. The measurements revealed basic estimates of sediment production and detailed spatial and temporal patterns of the valley bottom sediment in the headwater channel.



Fig. 8.2 Artificial check dams in the Ohya-kuzure landslide along a tributary of the upper Abe-kawa River. Quite many dams have been constructed for “sabo” erosion control work in this area. The entire photograph shows a part of the area of the Ohya-kuzure landslide terrain, and the study site, the Ichino-sawa catchment, is shown in the central left of the photograph

8.2 The Ohya-Kuzure Landslide Site

The Ohya-kuzure landslide is located in the upstream part of the Abe-kawa River watershed (Fig. 8.3). The landslide is one of the largest non-volcanic landslides in Japan, having an area of 1.8 km² and an estimated volume of 1.2×10^8 m³ (Imaizumi et al. 2006). The landslide was triggered by an intense earthquake in 1707, the Hōei Earthquake, which had an estimated magnitude of M8–9 (Ishikawa 2011). Subsequently, the unstable landslide terrain has been one of the most active debris flow areas in Japan (Imaizumi et al. 2005, 2006).

The specific area selected for the TLS measurement is a midstream portion of a small headwater catchment named Ichinosawa (area: 0.22 km², channel length: 650 m) located in the north-central part of the Ohya-kuzure landslide (Figs. 8.2 and 8.3). This headwater catchment typically has a slope angle of 40–50°, which is greater than the angle of repose of the sediments. Hence, rock fragments from the hillslope bedrock, composed of a well-deformed accretionary complex including shale and sandstone of early Eocene to early Miocene age (Sugiyama and AIST 2010), readily reach the valley bottom forming talus deposits. Together with large quantities of gravel, boulders over several meters in diameter often accumulate in the steep – mostly over 30° – channel bed. Some surface water runoff regularly occurs but most of the water passes through the thick sediments as underground

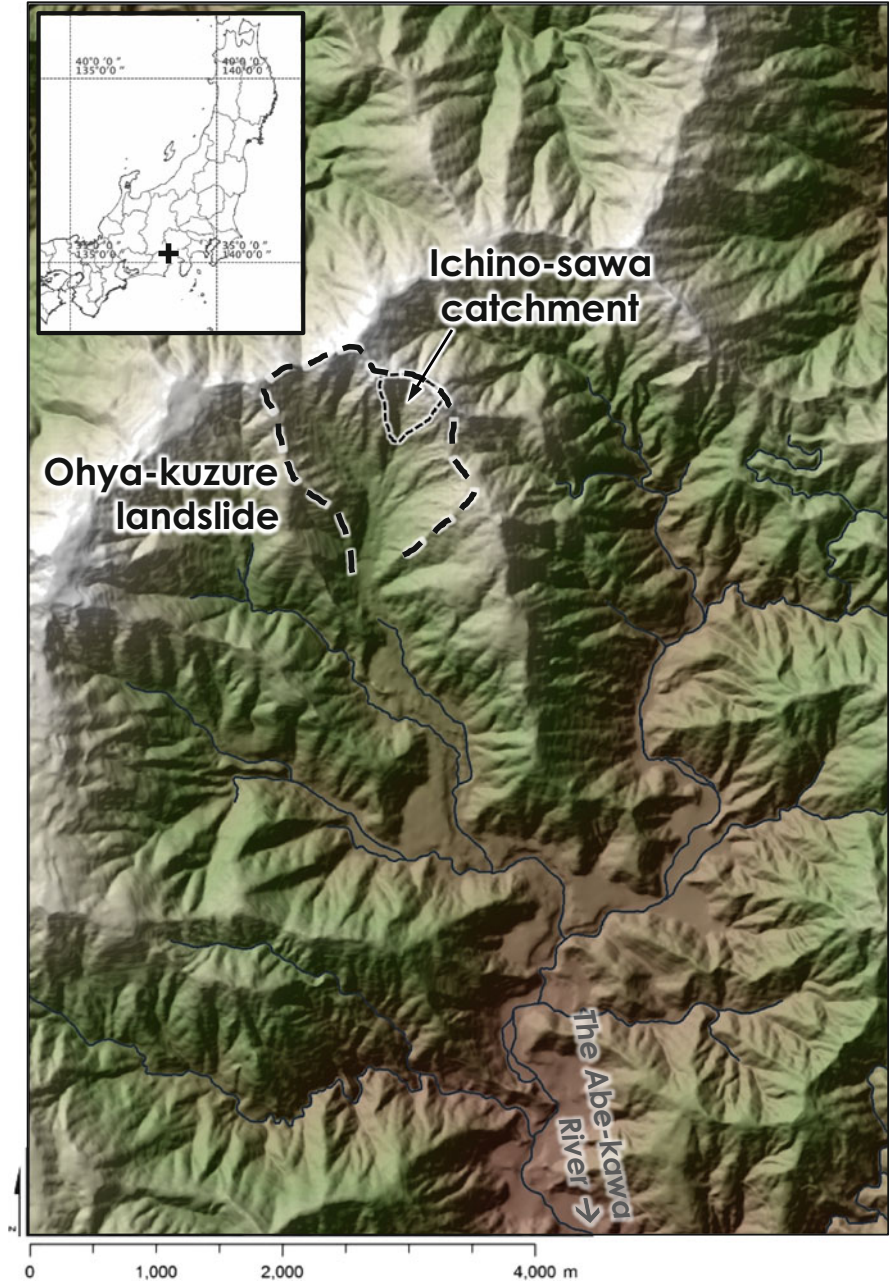


Fig. 8.3 Topography around the Ohya-kuzure landslide, the background hillshade image is derived from a 10-m DEM provided by Hokkaido-Chizu Co.

flow. Due to the frequent disturbance of the steep bedrock slopes, vegetation cover is limited and the slopes are bare rock surfaces.

The annual precipitation in the study area is ca. 3400 mm. Rainfall is seasonal and occurs mainly in the wet season from June to October, when the effects of cold fronts and typhoons are active; precipitation from December to February accounts for just 10 % of annual totals (Imaizumi et al. 2006). The catchment was significantly scoured during the summer of 2011 and the amount of valley-bottom sediment was observed to be the smallest in the last decade. November 2011 was therefore the appropriate time for the commencement of continuous field measurement.

8.3 Methods

A GLS-1500 terrestrial laser scanner by Topcon Co., Japan (Fig. 8.4) was used for the measurements of the valley floor. The maximum measurable range of the scanner is 500 m (for target objects with a 90 % reflectance), with accuracies of 4 mm in distance (at 150 m range) and 6'' of angle. The minimum point spacing is 1 mm at 20 m distance; the spot diameter of the laser is approximately 16 mm at a distance of 100 m. Because an infrared laser with a wavelength of 1535 nm was used in the device, the laser scanning was inapplicable to water and wet materials. Atmospheric conditions, particularly moisture and fog, also strongly affect the capability of laser scanning. Measurement speed is up to 30,000 points per second, while the time for one scanning operation at a given position, including setup, object scanning, target marker measurement and photograph (RGB colour) capture, was approximately 40–80 min. The body weight of the device is 16 kg (without batteries), and the total weight including other necessary items (battery, tripod, operation computer, targets etc.) is 40–50 kg.

Beginning in November 2011, field measurements were carried out in spring (May), summer (August), and autumn (November) for 2 years (Table 8.1). The time series of TLS data obtained during a total of seven seasons were labelled as: 1111, 1205, 1208, 1211, 1305, 1308, and 1311, where each number shows the year in two digit form followed by the month.

For each measurement, the scanner was set at two positions, on the downstream and upstream sides of the target area (Fig. 8.5). The scan position on the downstream side was located on a bedrock slope, where the land has been relatively stable for many years. Some other monitoring equipment including a rain gauge and video cameras were also installed around this point. Because the stable area for placing the scanner is limited, the locational variation in the downstream scan position was relatively low each time (several meters of differences). In contrast, the location of the upstream-side scan position varied more, because it was set in the valley bottom where the surface morphology is very dynamic. There was therefore no fixed stable location for the scan position on the upstream side.



Fig. 8.4 Terrestrial laser scanner used in this study, GLS-1500 by Topcon Co.

Table 8.1 Conditions of the study site for each time of scanning

Number	Name	Date of survey	Sediment situation	Debris flow
1	1111	Nov-22-2011	Poor	–
2	1205	May-14-2012	Rich	–
3	1208	Aug-23-2012	Poor	Occurred
4	1211	Nov-21-2012	Very poor	Occurred
5	1305	May-10-2013	Rich	–
6	1308	Aug-16-2013	Still remains	–
7	1311	Nov-19-2013	Poor	Occurred

In order to perform registration of the point clouds, measured from different scan positions, at least five reference targets (markers with a special reflectance pattern for GLS-1500) were placed in the study area. The two point clouds obtained from the upstream and downstream scan positions were registered by the target matching (tie-point) method using these multiple reference targets. In addition, two further targets were set for georeferencing, i.e., registration onto geographic coordinates. Because the scanner was set with strict horizontal constraints, only XY transformation is necessary for the georeferencing, and hence two targets were considered to be enough. The positions of the georeference targets were measured with GNSS (global navigation satellite system) receivers (Topcon GRS-1 or Trimble GeoXH 6000) which are capable of obtaining geographic coordinates with horizontal and vertical accuracies of <math>< 10\text{ cm}</math> by post-processing corrections. The baseline solution was obtained using the public data of nearby GNSS base stations provided by



Fig. 8.5 Target area for terrestrial laser scanning. The background hillshade image is derived from an airborne-laser derived DEM with a resolution of 1 m provided by MLIT. Transverse cross section lines (20 m long) are set along the longitudinal section of the valley centre (170 m) at a spacing of 5 m. Two *white circles* indicate the approximate scan positions of the TLS. *Arrows* show the flow directions of major channels

GEONET, the Japanese GNSS network operated by the Geospatial Authority of Japan.

Point cloud data were obtained and managed using Topcon ScanMaster software. The point cloud data were first georeferenced onto geographic coordinates (Japan Plane Rectangular CS VIII with JGD2000 datum, EPSG:2450) by distance resections using the two georeference targets coupled with the GNSS coordinates. After manually eliminating unnecessary points or noises, the point clouds were exported as a LAS file and imported into ESRI ArcGIS software. The point clouds were then converted into DEMs by using simple triangulated irregular network (TIN) interpolation, because minimal vegetation cover was present. The resolution of the DEMs was set, according to the average point density of the point clouds.

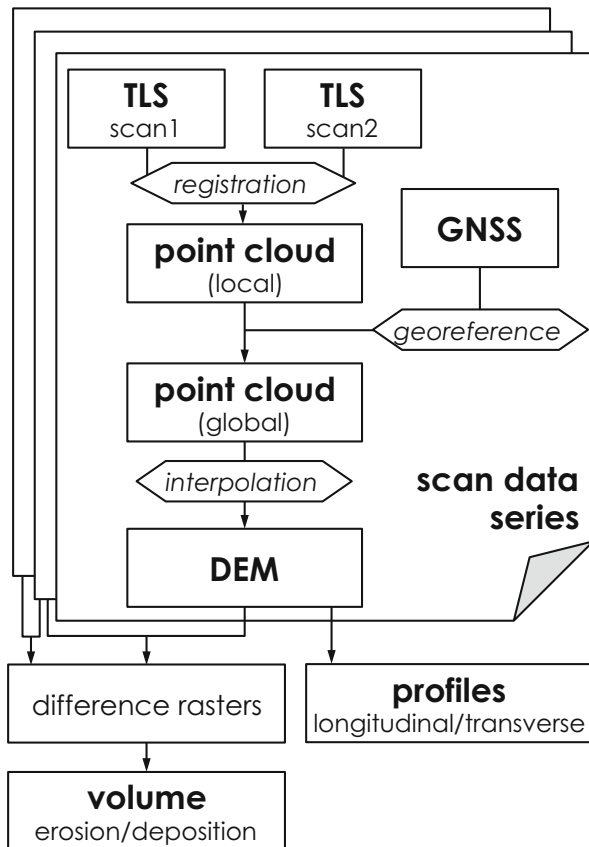
Differences of the DEMs between closest time periods were then computed (labelling rule: e.g., 1205–1111). A DEM with a resolution of 1 m obtained by airborne laser scanning (ALS) in 2010, provided by a local office of the Ministry of Land, Infrastructure, Transport and Tourism of Japan (MLIT), was also used to represent the initial condition of the study area. Sections for longitudinal and transverse profiles were set for the valley bottom sediment, covering areas 170 m long and 20 m wide (Fig. 8.5). The spacing of the transverse cross-sections was 5 m. Elevation along the profiles was then extracted, and the temporal changes in the profile elevation compared. Channel slope gradients were also calculated along the longitudinal profiles, using a measurement scale of 6 m which averages the very local variations in slope gradient caused by individual boulders. Although the elevation of bedrock beneath the sediment is difficult to establish in many parts of the study reach due to the thickness of coarse sediment, the approximate amount of sediments therein was quantified by subtracting the minimum elevation of DEMs throughout the time periods from each DEM. This is referred to as the depth raster of the valley bottom sediment. From the depth raster, the volumes of sediment within the study reach can then be calculated. The method is summarized as a workflow chart in Fig. 8.6.

8.4 Results

After field measurement and data processing, point clouds of the target area were obtained (Fig. 8.7). The registration errors, i.e. errors related to the target-based matching of two point clouds for each day of scan, were typically of the order of millimeters, while georeferencing errors which relate to the coordinates measured with GNSS receivers were of the order of centimeters (estimated accuracies of the post-processed GNSS data were <10 cm). In addition, the measurement error by TLS is of the order of millimeters (4 mm at 150 m distance, as noted before). The overall accuracies of the point clouds obtained are therefore considered to be of the order of centimeters to a decimeter.

Table 8.2 shows the properties of all point clouds obtained. Depending on the measurement conditions at the field site (mostly a factor of atmospheric condition,

Fig. 8.6 Data processing workflow in this study



for example in some cases the sudden occurrence of fog disabled the laser measurement), the total returned number of laser scans varies from 2,349,712 to 16,107,191 points. The density of point clouds, i.e. the number of points normalized by scan area, ranges from 62.0 to 306.0 points/m². These values equate to a mean spacing between points of between 0.062 and 0.127 m. The resolution of DEM converted from the point cloud was therefore determined to be 0.1 m for all the scan data.

At the beginning of the TLS surveys in November 2011, the sediment present in the study site was much less compared with that in the previous years, according to visual observations in the field. Although resolutions are different, the difference between the 10-cm DEM of the TLS data (1111) and the 1-m DEM of ALS taken in 2010 clearly shows there was sediment missing in 2011 (Fig. 8.8a). In many areas, changes in bed elevation of more than 5 m were observed. Figure 8.9a illustrates the estimated changes in the bed elevation in the study reach.

In some periods, particularly 1211–1305 (Fig. 8.8e), the trend of positive and negative changes in elevation (slightly over ± 40 cm) is different for each side of

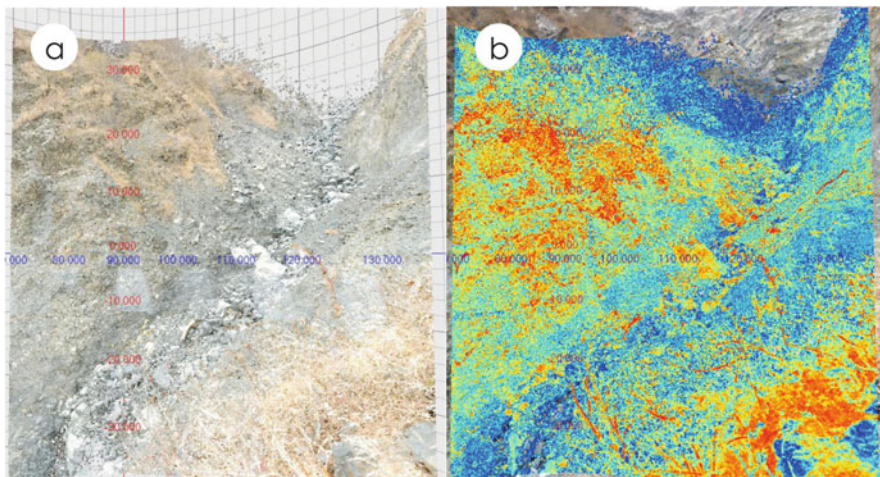


Fig. 8.7 Point cloud data obtained by TLS measurement (1111). (a) RGB-colour coded points, reproducing three-dimensional structure of visible scenery. (b) Point cloud coloured by intensity values of laser returns (*red*: high, *blue*: low). The intensity values are mostly high in surrounding steep slopes where intense laser returns are expected due to the angle of surface to the laser emission

Table 8.2 Point cloud properties of each scan

Name	Date (YY/MM/DD)	Total returns (pts)	Area of point cloud (m ²)	Shot density (pts/m ²)	Equivalent resolution (m)
1122	11/11/22	2,349,712	26,223	89.6	0.106
1205	12/05/14	3,541,973	40,891	86.6	0.107
1208	12/08/23	6,802,080	37,337	182.2	0.074
1211	12/11/21	16,107,191	52,641	306	0.057
1305	13/05/10	3,547,361	57,200	62	0.127
1308	13/08/16	12,303,233	47,000	261.8	0.062
1311	13/11/19	8,008,954	40,100	199.7	0.071

the valley-side slopes: positive elevation change dominates on the left-side slope while negative change dominates on the right-side slope (Fig. 8.8e). Because the slope gradients of the valley sides are quite steep (typically 30–80°), unexpected slight lateral shifts of the data (horizontal error) can easily affect the vertical changes for such steep slopes. These systematic variations in elevation difference, for the entire side slopes, are likely to be due to such lateral shifts of the data caused by errors in georeferencing, and these particular trends have been disregarded. Distinct local changes in elevation can be observed despite such overall trends. Hereafter these localized changes in elevation between each scan are described.

Following the winter season of 2011–2012, the amount of sediment in the study reach generally increased, and the difference between 1111 and 1205 in the TLS data indicates a marked deposition in upstream and downstream portions of the

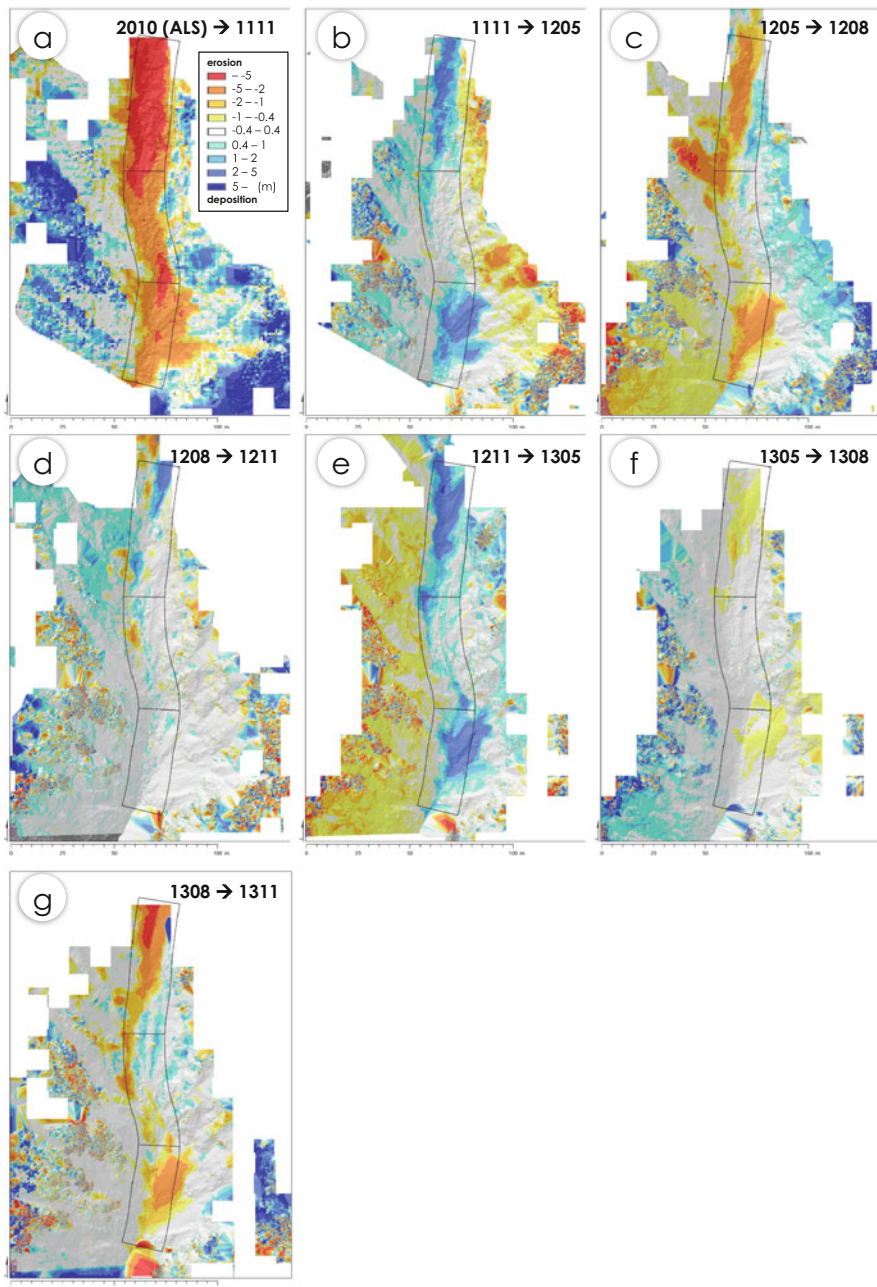


Fig. 8.8 Differences of elevation for each season. Areas with insufficient point data are masked by white cells. (a) 1111 compared to ALS data (1 m resolution) in 2010. A large amount of erosion of the valley bottom sediment is clearly observed. (b) 1205 compared to 1111. Deposition is observed in the upstream reach and the downstream talus cones. (c) 1208 compared to 1205. Erosion is occurring. Slope collapse has occurred in the right side slope at the mid-upper position. (d) 1211 compared to 1208. Relatively less changes are observed, while some patchy erosion is

study reach of more than 2 m depth (Fig. 8.8b). The depositional areas are mostly due to the development of talus cones, the sediment of which is supplied from side slopes (Fig. 8.9b).

During the rainy season, from 1205 to 1208, several debris flows occurred, and the erosion of the deposits appears to have taken place in the study reach (Fig. 8.8c). The right bank in the mid-section of the study reach showed a typical negative change in elevation, which corresponds to the collapse of bedrock on the valley-side slope (white dashed line in Fig. 8.9c).

During the transition from the summer to autumn season (1208–1211), the overall changes in elevation appear to have been less than those of the previous seasons, where almost no change was observed for the lower portion of the study reach. However, in the mid to upper sections, patchy erosion was observed (mostly on the right-side bank), while deposition occurred in the uppermost section of the study reach (Figs. 8.8d and 8.9d).

Through the following winter (1211–1305), deposition occurred again mainly in the upper and lower parts of the study reach (Fig. 8.8e). The area of deposition appears to have been slightly larger than that in the previous year (Fig. 8.8b). However, despite the dominance of deposition, two linear depressions along the flow direction were observed on the surface of the deposits in the mid reach (Fig. 8.9e), indicating some surface erosion.

During the period 1305–1308, no heavy rainfall events were recorded and changes in the sediment elevation were minor except for slight erosion in the upper portion and lower talus cone in the study reach (Fig. 8.8f). The surface sediment appeared to be somewhat coarser than in the spring season (Fig. 8.9f).

In the summer of 2013, heavy rainfall occurred several times during typhoon events and multiple debris flows were observed in the study reach. The amount of erosion was accordingly large during this time period (1308–1311) (Fig. 8.8g). In some portions in the upper part of the valley, bottom sediment was subject to more than 5 m of erosion, whereas linear areas of deposition along the flow direction were observed on the left side of the mid reach (Figs. 8.8g and 8.9g).

As noted above, the surface elevation of the valley bottom sediment is generally at a minimum in summer and at a maximum in spring. However, the changes differ locally within the study reach. The longitudinal profiles along the study reach, whose average slope is as steep as 54 %, clearly show contrasting trends of erosion and deposition (Fig. 8.10a). The upper and lower sections have large changes in elevation, while the middle section shows much smaller changes. Compared to the summer data (1208) when the bed elevation was nearly at its minimum (Fig. 8.8c), the deposition through winter was much more, 2–3 m in the lower section and up to



Fig. 8.8 (continued) observed at the right side in mid to upper portions. Clear deposition is shown in the uppermost position. (e) 1305 compared to 1211. Deposition is clearly observed. (f) 1308 compared to 1305. Less changes are observed, except some erosion in upstream and downstream portions. (g) 1311 compared to 1308. A high amount of erosion is observed in the upstream reach, while some deposition is also shown in the mid reach

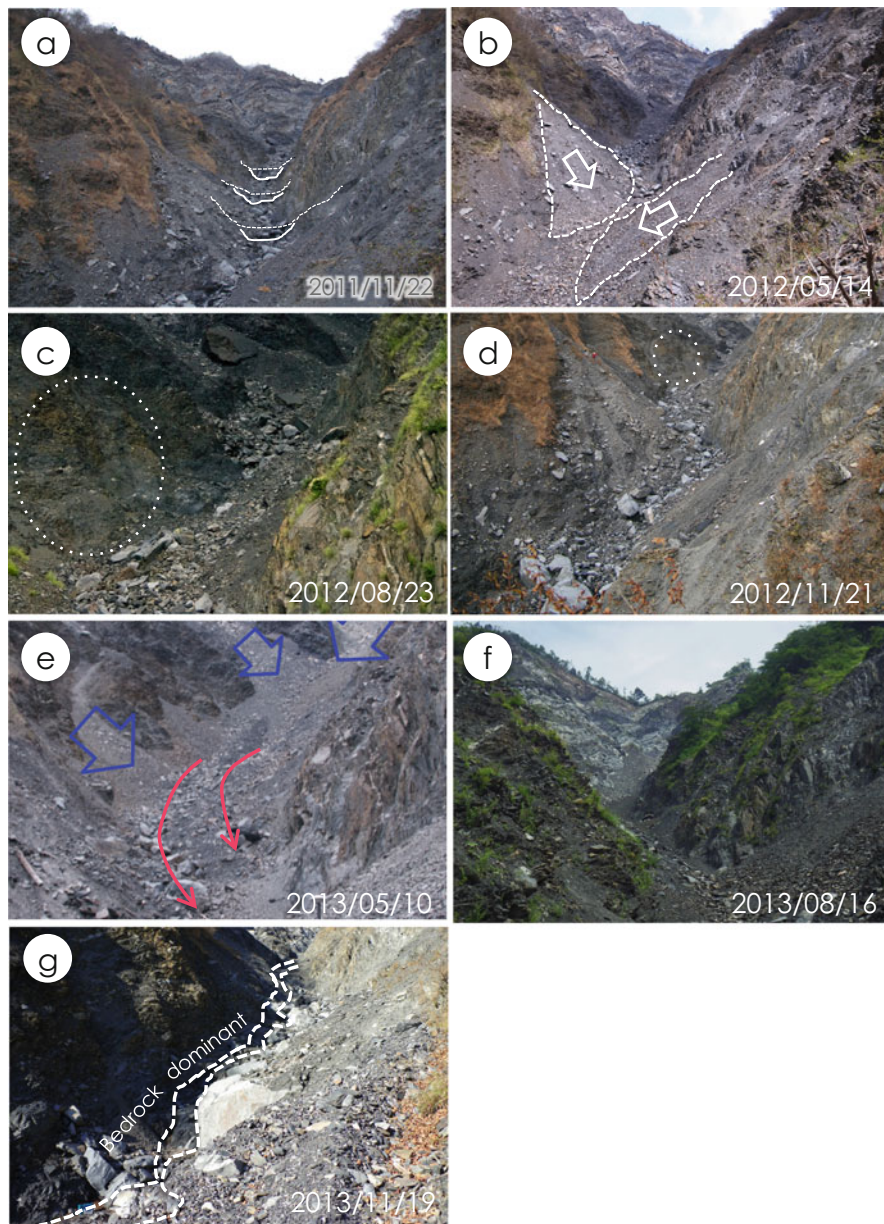


Fig. 8.9 Pictures of the scan target area for each survey. (a) 1111. Approximate cross-sections in 2010 are shown in white dashed lines. (b) 1205. Talus cones are clearly observed in the downstream part of the study reach. (c) 1208, zoom-in view of the mid to upper portions. *White dashed circle* indicates the location of slope collapse on the right side slope (see Fig. 8.8c). (d) 1211. The *dashed circle* corresponds to that in (c). (e) 1305. Sediments supplied from side slopes (*wide blue arrows*) are abundant, whereas erosional lineaments are also observed (*thin red arrows*). (f) 1308. The situation is similar to 1305. (g) 1311. The sediments have been well eroded, and bedrock surfaces are well observed

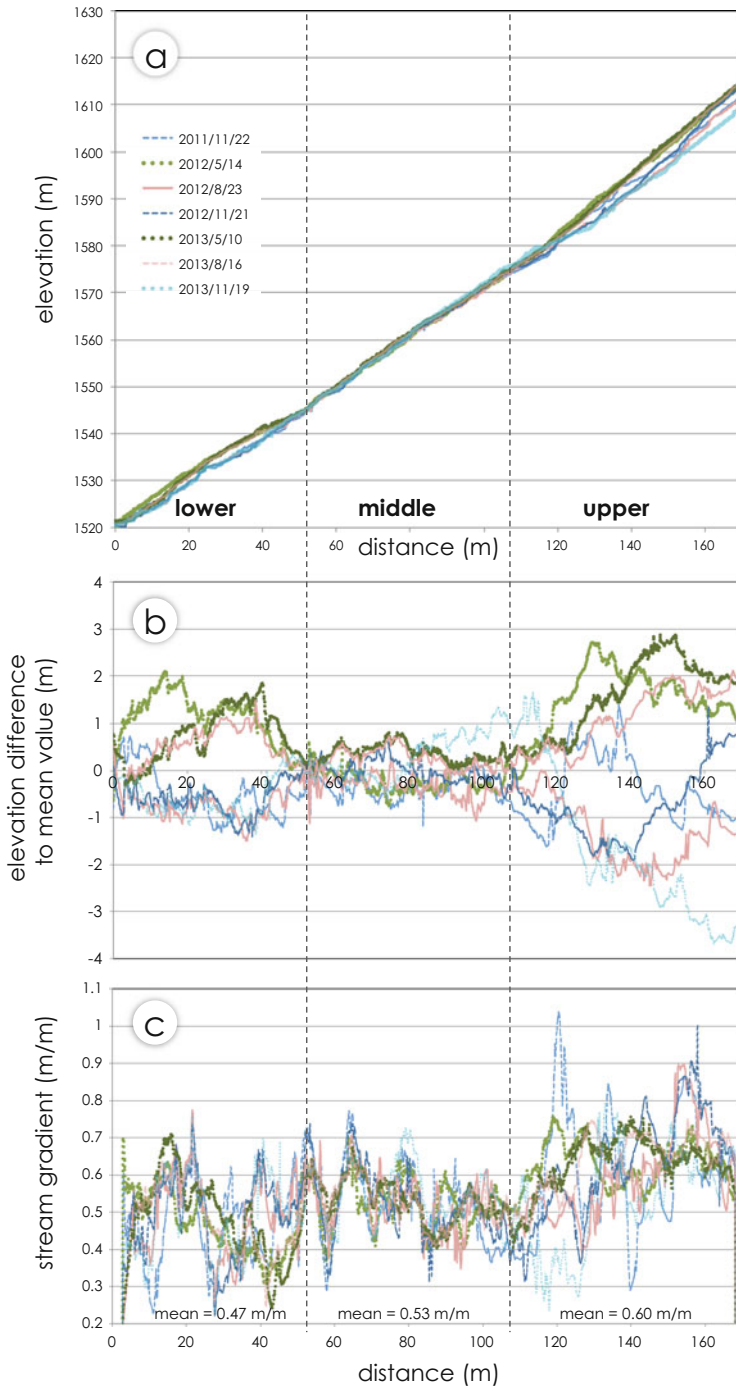


Fig. 8.10 (a) Longitudinal profile of the study reach for each season. (b) Seasonal differences in elevation, normalized by the mean elevation value for the entire datasets. (c) Stream gradient

5 m in the upper section, while the changes in the middle section only show ± 1 m differences (Fig. 8.10b). The upper section also showed greater deposition (1–3 m) before winter. These three subsections, i.e., the lower, middle and upper sections, can then clearly be separated according to these observations. Hereafter these domains are referred to as the upper, middle and lower sections, respectively. By extracting the watershed boundaries from the 1-m DEM by ALS, the source area above the uppermost point in the study reach appears to be 80,353 m², and the catchment areas feeding from side slopes into each section are 51,678 m² for the upper, 17,268 m² for the middle, and 27,487 m² for the lower one.

The 6-m scale stream gradients show cyclic patterns along the valley (Fig. 8.10c), which is more distinct in summer to autumn. These peaks in stream gradient represent both coarse sediment (boulders) and bedrock knickpoints. The cyclic pattern of the gradient, which changes seasonally, indicates step-pool-like features in the valley bottom sediment, presumably related to the pulses of debris flows and/or hydraulic forces by surface flows over the deposits. The boundaries of the subsections, in contrast, correspond to the locus of bedrock knickpoints with the fixed locations of the high peaks of stream gradient.

Transverse cross profiles also show the contrasting differences in bed elevation along the study reach (Fig. 8.11). The upper section shows clear deposition through winter, as well as slight deposition before winter (Fig. 8.11a, b). Some parts of the middle section show large changes (~ 2 m) (Fig. 8.11c) but typically less (< 1 m) (Fig. 8.11d). The lower section shows 2–3 m of deposition through winter, but is less dynamic in other seasons (Fig. 8.11e, f).

By subtracting the minimum elevation raster from each DEM, the temporal changes of the sediment storage were obtained, and found to be 1000–5000 m³ (Fig. 8.12). As noted above, sediment storage is generally high in spring and low in summer, but local variations indicate that the storage in the middle section is relatively stable throughout the seasons.

8.5 Discussion and Conclusions

The order-of-magnitude estimate of sediment storage within this reach corresponds well with the sediment volume of 2000–19,000 m³ in a longer reach, including that of this study, roughly estimated by photographs for an older time period (2001–2004) (Imaizumi et al. 2006). This indicates that, with some variations, the sediment yield in the study area has been consistently high (in the order of 10^3 – 10^4 m³) for years to decades. However, even along the short reach of the scan area, the three subsections exhibit different patterns of erosion and deposition of sediment. Such local variations can be related to those variations occurring in debris flow

Fig. 8.10 (continued) (horizontal scale: 6 m) for each season. Mean values of stream gradient for each subsection are also shown

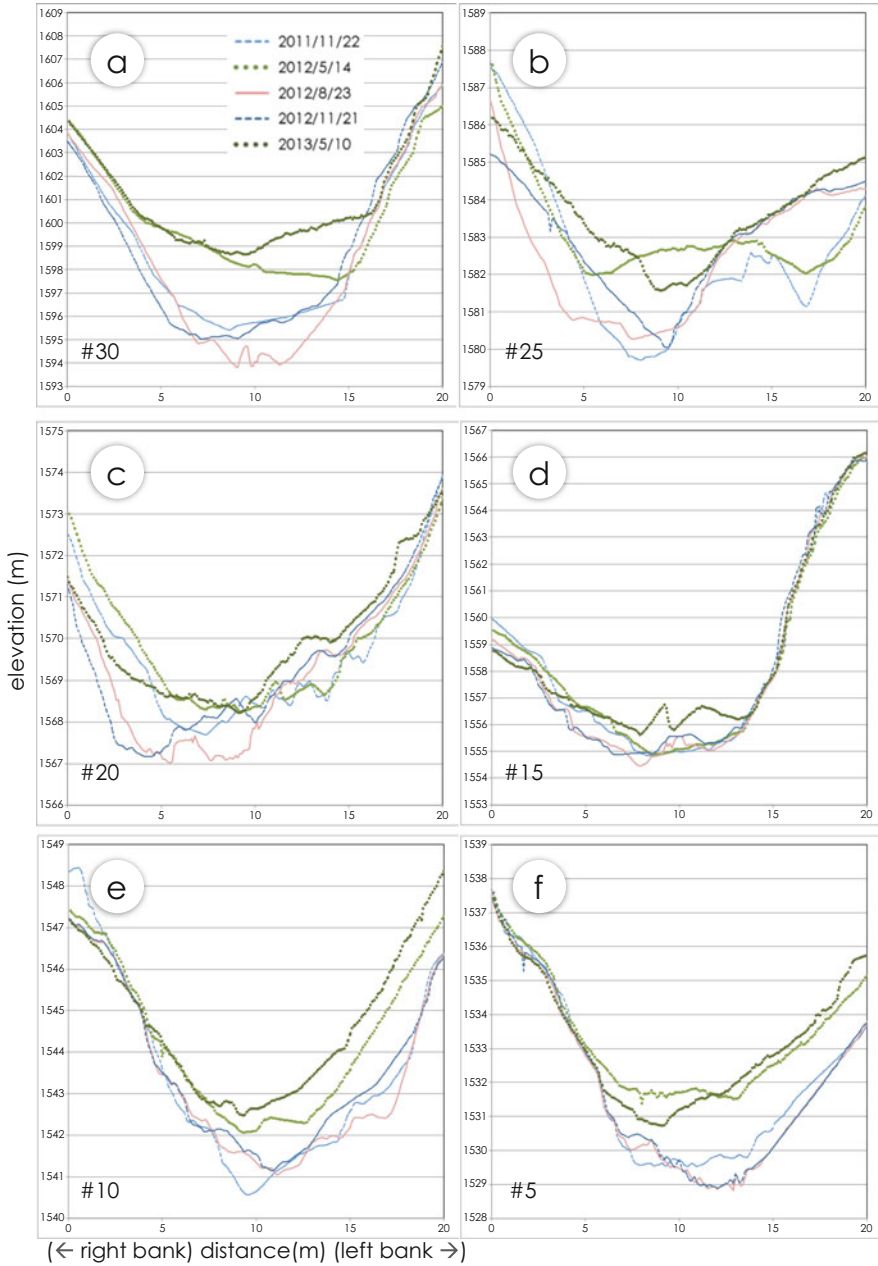


Fig. 8.11 Examples of transverse cross profiles along the study reach. Number of section lines is shown in Fig. 8.5

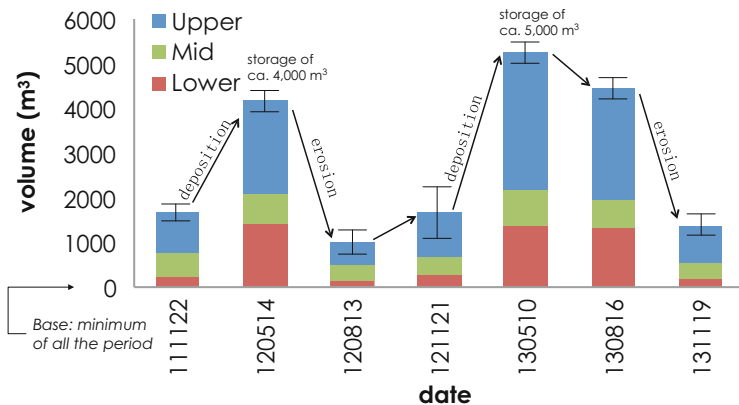


Fig. 8.12 Seasonal changes in sediment storage in the target area

dynamics and surrounding topographic conditions. The boundaries between the subsections (Fig. 8.10) seem to correspond to the narrowing portions of the valley where distinct bedrock exposure on the valley bottom occurs as knickpoints. The bedrock topography of the valley bottom and valley-side slopes can therefore be important in determining the kinematics of debris flows therein. Also, the bedrock in the valley bottom itself can change by erosion when exposed to the debris flowing over it. The bedrock of the valley-side slopes actually changed due to a collapse event (Figs. 8.8c and 8.9c), which acted to widen the valley. The interactions between debris flows and bedrock will change the location and characteristics of the subsections on a decadal time scale.

The upper section appears to have experienced the largest changes and variability in topography. Here, the slope gradient is steepest and the sediments could have a higher mobility than those of the lower sections. Transportation of both fine and coarse sediments may occur by recurring debris flows in this section. However, monitoring of the debris flows in this section is limited because of the fact that video recordings for this section were not possible. Judging from the predominantly coarse sediments in this section, relatively infrequent, intense debris flows are likely to be responsible for the higher mobility of valley bottom sediments here.

The middle section exhibits considerably less change in surface elevation compared to the upper and lower sections. The downstream end of this section, which corresponds to the point where the valley narrows and bedrock exposed as a knickpoint, may have a higher water depth during flooding. Increased shear stress, induced by surface flows, could lead to a greater mobility of finer-grained sediments (small gravels), whereas this is not sufficient to mobilize larger boulders lying beneath the finer material.

In the lower section, the supply of relatively fine-grained sediments from the valley side slopes is abundant, and is observed as large talus cones on both sides of the channel. In this reach, remobilization of fine sediments by debris flows was captured by video monitoring (Imaizumi et al. 2013). Imaizumi et al. (2013)

observed that the prominent surface flow causes partial fluidification and mass movements of channel bed deposits. Following the migration of the portion that was fluidized, the compaction of the finer sediments leads to frequent saturation and finally causes debris flows. By this mechanism, the majority of mobile particles during debris flows are fine-grained sediments rather than large boulders. As shown in the longitudinal profiles (Fig. 8.10), the changes in sediment elevation are moderate in this section, and field observation shows that the changes are mostly due to the accumulation and removal of relatively fine-grained sediments, while large boulders seem to be immobile and only excavated following debris flows (Fig. 8.9). Relatively low stream gradients in this section (0.47 m/m) may account for the fact that debris flow energies are insufficient to initiate the movement of larger sediment blocks.

The source of the sediment in each subsection can be divided into two types: (1) small to large sediment particles transported from the upstream area by debris flows, and (2) small particles supplied from the side slopes. The latter is mostly derived from freeze-thaw weathering of the surrounding slopes composed of deformed shale and sandstone layers, which provide small rock particles into the valley bottom, particularly in the late autumn to early spring season.

The uppermost catchment above the study reach has an area of 80,353 m², and this seems sufficient for the accumulation of enough surface water to generate debris flows when intense rainfall events occur; large boulders can then be transported by such debris flows along the valley bottom. The side slopes along the upper section also have relatively large catchment areas (51,678 m² in total), and such areas are, even though clear channels are not apparent, favourable for the abundant supply of sediment by mass movements onto the valley bottom. This source of sediment supply is responsible for the high amount of deposition and erosion in the upper section throughout the year.

On the contrary, the side slope source areas for the middle section are relatively small (17,268 m²), and the sediment supply into this section relies mainly on debris flows coming from the upper section. Due to the narrowing of the valley and associated knickpoint at the downstream end of the middle section, sediments coming from upstream can be trapped at this point and maintain a valley bottom surface that is smoother than the underlying bedrock. This sediment cover may be the cause of the small range of fluctuations in valley-bottom elevations in this section: the transported sediments can pass over the relatively smooth surface, and neither erosion nor deposition occurs within this reach to any significant degree. In addition, the narrowness of the valley may cause a significant increase in water depth during flooding, and the consequent higher shear stresses developed would be expected to make sediment mobilization easier.

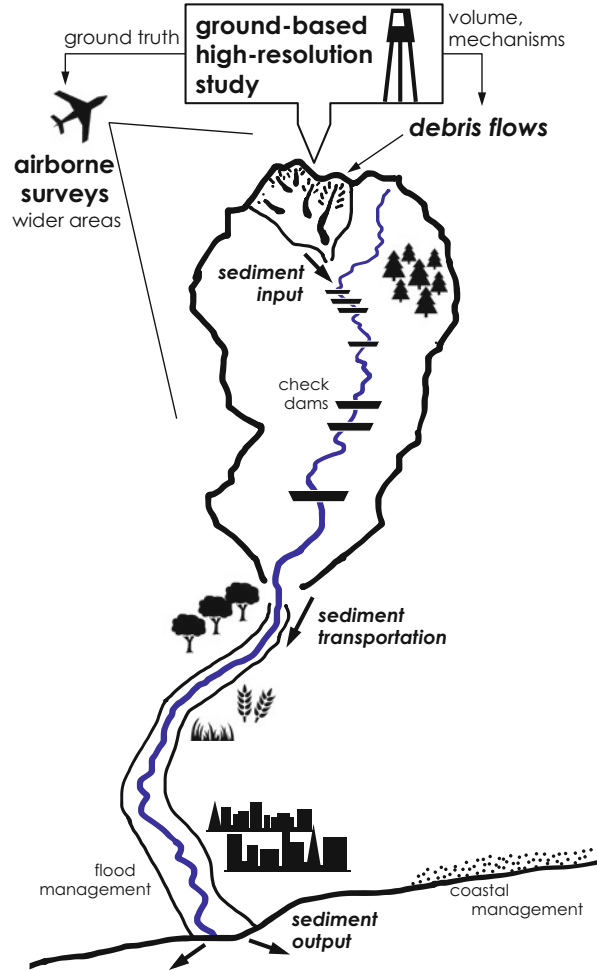
Sediment input from the side slopes is again large in the lower section, with a total source area of 27,487 m², where obvious talus cones are observed. In addition, due to the increased volume of water in this downstream reach, sediment delivered by debris flows can readily travel further downstream once initiated. Accordingly, the amount of deposition and erosion in this section is moderate compared to that of the upper section.

In summary, the TLS measurements of the debris-flow deposits in the valley bottom of the steep headwater channel in spring, summer and autumn over 2 years provide multi-temporal high-definition (0.1 m resolution) topographic datasets, revealing seasonal variations in the amount of valley-bottom sediment of the order of 1000–5000 m³. Erosion and deposition along the reach also shows contrasting spatial patterns according to the sections bounded by knickpoints and valley narrows. The upper section exhibits steepest channel slopes with the largest changes in valley-bottom elevation, indicating the more frequent transportation of coarse sediments. In the middle section, bed elevation is relatively constant, where transportation seems dominant due to smooth sediment coverage and deeper water flows within the narrow valley. In the lower section, immobile coarse boulders are present, while deposition and erosion of relatively fine sediments seem dominant.

It should be noted that even three centuries after the formation of the megalandslide, such disturbance regularly continues in the steep headwater catchment. The time period of this study is, however, relatively short (two years) compared to the entire history of this landslide terrain. Therefore, further monitoring and measurements should be, on one hand, continued to reveal longer-term, annual to decadal trends in sediment dynamics in the study site. On the other hand, linking such a high-resolution but short-term analysis on sediment production in the steep headwater channel to longer-term studies of sediment transport in broader areas is essential for comprehensive understandings of intense sediment transport from headwater to downstream (e.g., Korup et al. 2004).

Such long-term studies in downstream gentler reaches may include different approaches. Figure 8.13 shows a schematic illustration of sediment production and delivery in a watershed-scale area for the Abe-kawa River. The high-resolution ground-based survey, which provides detailed insights into volume, timing and mechanisms of sediment production by debris flows therein, can be used as a ground truth for aerial surveys, including aerial photogrammetry and ALS. The aerial survey has been carried out every year recently for a wider area of the Abe-kawa River catchment. Although the resolution by such aerial surveys is relatively low (1 m), compared to those by TLS (0.1 m), spatial analysis of the sediment transport by debris flows can be performed for broader areas in the catchment with a longer time span (e.g., Imaizumi et al. 2015), where TLS data may be used for assessment and enhancement of accuracies of the airborne data. Furthermore, the amount and local-scale characteristics of sediment deposition and erosion by debris flows in such a headwater steep channel should be related to the sediment yields in downstream areas. Although each debris flow in the study area mostly remains in the valley bottom of the landslide terrain and coarse sediment does not reach further downstream at annual scales (Imaizumi et al. [in press](#)), decadal transport rates of fine-grained and suspended sediments are constantly high in the downstream reach of the study area (Nishikawa et al. 2006; Kondo et al. 2008). Links between the timing and amount of mobile sediment production by upstream debris flows and sediment transport in the downstream reaches should therefore be further assessed. For instance, intense sediment yields, initially mobilized by debris flows and subsequently by fluvial transport, toward downstream

Fig. 8.13 Schematic illustration of issues on sediment dynamics in a watershed



reaches may be reduced by construction of numerous check dams along the reach. However, the decrease in sediment transport in the midstream of the river would result in bank erosion and damages in bridge piers. In contrast, downstream reaches of the Abe-kawa River shows a trend of increasing riverbed height even decades after prohibiting the operation of gravel and sand mining (Ito et al. 1999), potentially increasing the flood risks therein. Even flood risk may increase when land subsidence occurs due to earthquakes in such channelized lowlands (e.g., Hughes et al. 2014), where the study area is prone to frequent earthquakes and tsunamis. Long-term changes in the amount of sediment output from river to coastal areas on the order of $10^5 \text{ m}^3/\text{year}$ (Uda et al. 1994) can also cause changes in the amount of sand storage at the coast, which may result in uneven changes of the coastlines including significant coastal erosion. Like those, long-term, comprehensive mitigation strategies for sediment-related disasters should be applied to a whole

watershed from headwater to river mouth. Therefore, for the watershed-scale balancing of sediment budget, high-resolution and high-frequency monitoring of sediment production in headwater areas would strongly contribute to optimize the distribution of facilities for sediment controls along the mid to downstream reaches.

Acknowledgements Our research is funded by the Research Grant by Sabo & Landslide Technical Center, and JSPS KAKENHI Grant Numbers 26292077 and 25702014. This study is a part of CSIS Joint Research #413. We thank S. Ishikawa, N. Yumen, H. Mori, H. Yoshida, and students from Shizuoka University for their assistance in the field survey.

References

- Higuchi S, Tsuchiya S, Ohsaka O (2012) Large sediment movement caused by the catastrophic Ohya-Kuzure landslide. *Chubu Forest Res* 60:105–108 [in Japanese]
- Hughes MW, Hughes MW, Quigley MC, van Ballegooy S et al (2014) The sinking city: earthquakes increase flood hazard in Christchurch, New Zealand. *GSA Today* 25(3):4–10. doi:[10.1130/GSATG221A.1](https://doi.org/10.1130/GSATG221A.1)
- Imaizumi F, Tsuchiya S, Ohsaka O (2005) Behaviour of debris flows located in a mountainous torrent on the Ohya landslide, Japan. *Can Geotech J* 42:919–931
- Imaizumi F, Sidle RC, Tsuchiya S et al (2006) Hydrogeomorphic processes in a steep debris flow initiation zone. *Geophys Res Lett* 33:L10404. doi:[10.1029/2006GL026250](https://doi.org/10.1029/2006GL026250)
- Imaizumi F, Tsuchiya S, Ohsaka O, Ito H (2013) Surface runoff and fluidification of grains on sediment surface of sands and gravels. *Proc Jpn Soc Erosion Control Eng Annu Meet 2013: Pb–08* [in Japanese]
- Imaizumi F, Hayakawa YS, Hotta N et al (2015) Interactions between accumulation conditions of sediment storage and debris flow characteristics in a debris-flow initiation zone in Ohya landslide, Japan. *Geophys Res Abstr* 17:EGU2015–EGU7757
- Imaizumi F, Trappmann D, Matsuoka N et al (in press) Biographical sketch of a giant: deciphering recent debris-flow dynamics from the Ohya landslide body (Japanese Alps). *Geomorphology*
- Ishikawa Y (2011) Reevaluation of magnitude of Hoei earthquake in 1707 (in Japanese). *Abstracts of the seismology society of Japan 2011 Fall Meeting D11–09*. [in Japanese]
- Ito S, Ogawa Y, Sekiya Y et al (1999) On the sediment budget and bed variation of the Abe River. *Proc Hydraul Eng* 43:719–724. doi:[10.2208/prohe.43.719](https://doi.org/10.2208/prohe.43.719) [in Japanese with English abstract]
- Keefer DK (1999) Earthquake-induced landslides and their effects on alluvial fans. *J Sediment Res* 69:84–104. doi:[10.2110/jsr.69.84](https://doi.org/10.2110/jsr.69.84)
- Kondo R, Hashinoki T, Yasuda Y et al (2008) Observation of total load upstream of the Abe River. *Sabo Gakkaishi* 60(5):15–22. doi:[10.11475/sabo1973.60.5_15](https://doi.org/10.11475/sabo1973.60.5_15)
- Korup O (2012) Earth's portfolio of extreme sediment transport events. *Earth Sci Rev* 112:115–125. doi:[10.1016/j.earscirev.2012.02.006](https://doi.org/10.1016/j.earscirev.2012.02.006)
- Korup O, McSaveney MJ, Davies TRH (2004) Sediment generation and delivery from large historic landslides in the Southern Alps, New Zealand. *Geomorphology* 61:189–207. doi:[10.1016/j.geomorph.2004.01.001](https://doi.org/10.1016/j.geomorph.2004.01.001)
- Korup O, Clague JJ, Hermanns RL et al (2007) Giant landslides, topography, and erosion. *Earth Planet Sci Lett* 261:578–589. doi:[10.1016/j.epsl.2007.07.025](https://doi.org/10.1016/j.epsl.2007.07.025)
- Ministry of Construction (1988) History of sabo erosion controls in Abe-kawa River [in Japanese]
- Nishikawa T, Takahashi M, Kato Y et al (2006) Current status of suspended sediment measurements in the Abe-Kawa River. *Proc Jpn Soc Erosion Control Eng*. [in Japanese]
- Rowlands KA, Jones LD, Whitworth M (2003) Landslide laser scanning: a new look at an old problem. *Q J Eng Geol Hydrogeol* 36:155–157. doi:[10.1144/1470-9236/2003-08](https://doi.org/10.1144/1470-9236/2003-08)

- Sugiyama Y, AIST (2010) Geological map of Japan 1:200,000 Shizuoka and Omae-zaki, 2nd edn. Geological Survey of Japan, AIST [in Japanese with English abstract]
- Teza G, Galgaro A, Zaltron N et al (2007) Terrestrial laser scanner to detect landslide displacement fields: a new approach. *Int J Remote Sens* 28:3425–3446. doi:[10.1080/01431160601024234](https://doi.org/10.1080/01431160601024234)
- Trustrum NA, Gomez B, Page MJ et al (1999) Sediment production and output: The relative role of large magnitude events in steepland catchments. *Z Geomorphol Supplbd* 115:71–86
- Tsuchiya S, Imaizumi F (2010) Large sediment movement caused by the catastrophic Ohya-Kuzure landslide. *J Dis Res* 5:257–263
- Uda T, Suzuki T, Oishi M et al (1994) Evaluation of volume and spatial shape of beach sand along Shizuoka Coast. *Proc Coast Eng Soc Jpn* 41:536–540. doi:[10.2208/proce1989.41.536](https://doi.org/10.2208/proce1989.41.536) [in Japanese]